Marine and Petroleum Geology 48 (2013) 149–159

Contents lists available at ScienceDirect

Marine and Petroleum Geology

journal homepage: www.elsevier.com/locate/marpetgeo

Propagation of blind normal faults to the surface in basaltic sequences: Insights from 2D discrete element modelling

Stuart Hardy*

ICREA (Institució Catalana de Recerca i Estudis Avançats), Facultat de Geologia, Universitat de Barcelona, 08028 Barcelona, Catalonia, Spain

ARTICLE INFO

Article history:
Received 5 March 2013
Received in revised form
30 July 2013
Accepted 13 August 2013
Available online 22 August 2013

Keywords:
Normal faulting
Fracturing
Basalt
Simulation
Strain

ABSTRACT

A discrete element model is used to investigate the progressive deformation of a thin basaltic cover overlying a pre-existing, blind, normal fault as it propagates to the surface. The cover materials representing basalt are homogeneous, strong and display elastic-brittle material behaviour. Cover deformation is seen to evolve through a series of distinct stages. Initial displacement on the underlying fault produces a very gentle, monoclinal, flexure. With continued displacement, open fractures develop at the monocline surface and propagate downwards, whilst the deeper fault propagates upwards. Simultaneously, a series of fractures, in the future hanging-wall of the main fault, develop in the upper part of the cover. The monoclinal flexure is then cut by these structures, producing a surficial fault- and fracture-bounded wedge. Finally, a prominent surface fracture and the upward-propagating fault link, cutting the entire cover sequence. This fault is dilatant in the upper c. 100 m of the cover, has a significant surface aperture and forms a prominent fault scarp. Many of the key model results are strikingly similar to those seen in natural settings, and emphasise that the occurrence of dilatant faults, open fractures and cavities/caves in extensional settings is not necessarily restricted to the very shallow section but can extend to several hundred metres depth. Therefore, the results have implications for permeability and fluid flow in such settings. Comparison is also made with a weak cover experiment, using granular materials with no cohesion or tensile strength, similar to the dry sand used in many analogue modelling studies.

1. Introduction

Normal faults are of great importance in crustal evolution in a variety of tectonic settings (e.g., White et al., 1986; Gudmundsson, 1987; Leeder et al., 1991; Gawthorpe et al., 1997; Willsey et al., 2002; Martel and Langley, 2006) with field, laboratory and numerical modelling studies aiding our understanding of their geometry and development (e.g., Vendeville, 1988; Mandl, 2000; McClay, 1990; Withjack et al., 1990; Patton and Fletcher, 1995; Hardy and McClay, 1999; Sharp et al., 2000; Holland et al., 2006; Fig. 1a and b). As fundamental building blocks of rifts and continental margins, their geometries are of profound importance for topography, sediment pathways, petroleum migration and, more generally, for permeability and fluid flow. In addition to faults active at the Earth's surface, there are many examples where normal faults are buried beneath a cover of sediments (or lava flows) creating conditions in which a "blind" fault underlies intact cover materials which then deform with subsequent fault slip (e.g. Gawthorpe et al., 1997; Holland et al., 2006). However, due to a combination of lack of access or exposure, poor subsurface well control and limited seismic resolution, the relationships between deeper fault geometries, surface deformation and associated folding and fracturing in the cover are often not clear or well-constrained. This is particularly true for normal faults affecting basaltic sequences in active volcanic rifts, where surface exposure is often spectacular but deeper structure is obscured and poorly understood (e.g. Gudmundsson, 1987; Acocella et al., 2003; Martel and Langley, 2006; Holland et al., 2006).

There are a great many processes, at a variety of spatial and temporal scales, that contribute to the development of normal faults in basalts and their structural expression in nature. These range from grain-scale crack propagation, fracture development, individual seismic events that contribute to small increments of fault displacement (e.g., Ferrill et al., 2011), post-seismic slip and relaxation (Jónsson, 2008), to the growth and lateral propagation of large faults (e.g., Kaven and Martel, 2007; Villemin and Bergerat, 2013). However, regardless of the setting, there is abundant evidence that the style of normal faulting in basalts is quite distinctive: sub-vertical fault scarps, dilatant faults, open fractures, fissures and cavities/caves are common (e.g. Acocella et al., 2003; Martel and

* Tel.: +34 934 02 13 76.
E-mail address: stuart.hardy@icrea.cat.

0264-8172/$ – see front matter © 2013 Elsevier Ltd. All rights reserved.
http://dx.doi.org/10.1016/j.marpetgeo.2013.08.012

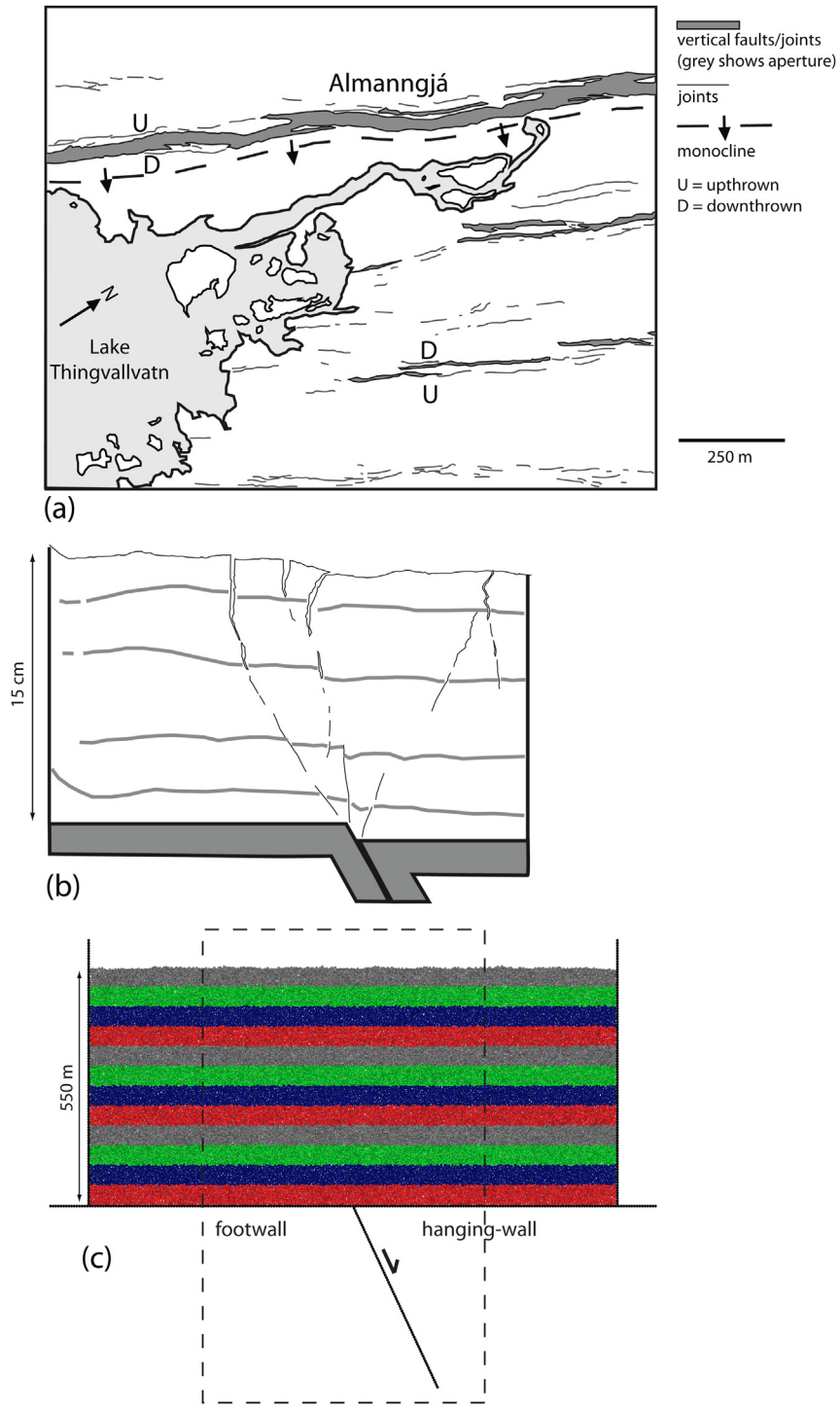

Figure 1. (a) Example of extensional faults developed in basalts from field studies, map of the Thingvellir fissure swarm in Iceland showing vertical, open faults and fractures (redrawn from Grant and Kattenhorn, 2004), (b) faults and fractures developed in an analogue model of normal faulting beneath a strong, cohesive cover material – hemihydrate powder (redrawn from Holland, 2004) and, (c) discrete element model setup used here showing initial and boundary conditions, central part of model illustrated in subsequent figures indicated by dashed box. See text for discussion.

Langley, 2006; Holland et al., 2006; Ferrill et al., 2011; Fig. 1a and b) in contrast to the near-surface deformation seen in typical sedimentary cover rocks. Surface opening magnitudes (apertures) of such fractures are typically several metres but those of the faults can be much greater, with values of up to c. 70 m being reported (cf. Gudmundsson, 1987; Acocella et al., 2003; Grant and Kattenhorn, 2004; Fig. 1a). However, the deeper geometry of these fault and fracture networks, and their evolution in 2D and 3D, is poorly known. In addition, there has been much discussion on the fundamental manner in which such faults develop, some authors advocating that they initiate as open fractures that propagate downwards from the surface (Acocella et al., 2003), while others favour a model in which a deep, blind fault propagates upwards (Grant and Kattenhorn, 2004; Kaven and Martel, 2007).

To investigate normal faulting, analogue (laboratory) models have frequently employed weak, granular materials (dry sand or

glass beads) to represent brittle rocks, and have produced results that bear a good, first-order, resemblance to many normal fault geometries observed in the upper crust (e.g. Horsfield, 1977; Vendeville, 1988; McClay, 1990). Depending on the setting being considered, granular materials with different frictional properties can be inter-layered, or underlain by viscous polymer layers etc, to produce a wide variety of mechanical stratigraphies which, when subject to boundary conditions appropriate for normal faulting, produce interesting and complex geometries (e.g. Vendeville, 1988; Dooley et al., 2003). However, most simple granular materials have inherent limitations in that they have no tensile strength, only a very small apparent cohesion and do not support open fractures or cavities (cf. van Gent et al., 2010). Clearly, this is a particular problem when considering near-surface faults developed in intact basalts or cemented carbonates. As a result, some authors have used cohesive powders, plaster, damp sand, sand–clay mixtures or clay to investigate deformation of such cohesive, stronger rocks (e.g. Withjack et al., 1990; Clifton and Schlische, 2003; Holland et al., 2006, 2011; van Gent et al., 2010; cf. Fig. 1b). Such materials may allow open fractures to develop, although the material properties (in particular the cohesion, tensile and compressive strengths) and scaling of such analogues are not always well-characterized.

Similarly, kinematic and geometric models based on flexural slip, inclined shear, trishear etc., have been widely used to predict/restore hanging-wall/footwall geometries and strain associated with normal faults with some success (e.g., White et al., 1986; Allmendinger, 1998; Hardy and McClay, 1999; Jin and Groshong, 2006; Withjack and Schlische, 2006). However, they are limited by their imposed kinematics and take no account of the evolving mechanical response of the deforming rock mass, predicting only continuous deformation and large-scale fold geometries. In addition, experimental and field evidence of cover deformation points to a structural evolution that is much more complex than that predicted by such geometric/kinematic models (e.g., Horsfield, 1977; Sharp et al., 2000; Jackson et al., 2006; Fig. 1a and b). In contrast, mechanical numerical models allow more realistic, complex rheologies (Mohr-Coulomb, elastoplastic, viscous, viscoelastic, etc) to be defined for the rock mass whereby the deformation of the cover in response to imposed boundary stresses or displacements can be assessed (e.g., Patton and Fletcher, 1995; Crook et al., 2006; Smart et al., 2010). However, whilst producing a detailed picture of evolving stress and strain, most mechanical models (e.g., finite element, viscous, boundary element) still do not reproduce the secondary structures, particularly the faults, open fractures, cavities/caves etc., seen in the field and laboratory. This is partly a result of the limitations of some numerical codes in modelling spontaneous localisation and large displacement on faults and, more generally, the continuum numerical techniques used not allowing cavities or open fractures to develop (cf. Crook et al., 2006; Nollet et al., 2012). In contrast, discontinuum techniques (such as the discrete element method or smooth particle hydrodynamics) allow natural fault localisation and propagation, can incorporate a variety of rheologies, and replicate the complexity of smaller scale structures (including cavities and open fractures) seen in the field and laboratory (e.g., Saltzer and Pollard, 1992; Gray and Monaghan, 2004; Hardy, 2008). They also allow a detailed analysis of kinematics and strain (e.g., Cardozo and Allmendinger, 2009; Hardy, 2011). It is the discrete element technique that will be used in the study presented herein.

Discrete element models have been used previously to examine deformation in cover materials above normal faults and have produced results similar to those seen in field and analogue modelling studies. However, these models have either treated the cover as elastic-brittle but frictionless (Finch et al., 2004), purely frictional (Egholm et al., 2007; Hardy, 2011) or have investigated the very early stages of cover deformation in cohesive materials in laboratory-scale (30 cm wide by 15 cm high) numerical and analogue models (Abe et al., 2011). Herein, I build on these studies by using a high-resolution 2D discrete element model to examine deformation of an intact, strong, basaltic cover overlying a normal fault, at a scale and final displacement similar to that observed at outcrop in active rift systems (cf. Acocella et al., 2003; Martel and Langley, 2006; Holland et al., 2006). The physics of individual seismic (slip) events on the basement fault are not considered in the model but rather the effect of cumulative displacement on this fault on cover deformation. The model focusses on a thin basaltic cover sequence (~550 m thick) and uses elements whose average radius is approximately 2 m – thus allowing a good resolution of small, secondary structures. The cover materials representing basalt are homogeneous, strong and display elastic-brittle-frictional material behaviour (cf. Finch et al., 2004; Hardy, 2011). Many of the key model results are strikingly similar to those seen in natural settings, and emphasise that the occurrence of dilatant faults, open fractures and cavities/caves in extensional settings is not necessarily restricted to the very shallow section but can extend to several hundred metres depth. Results are also compared to an experiment using granular cover materials with no cohesion or tensile strength, similar to the dry sand used in many analogue modelling studies.

2. Modelling methodology and boundary conditions

A series of discrete element numerical experiments have been conducted in order to better understand cover deformation in basaltic sequences, subject to boundary conditions which simulate deformation above a blind, normal fault propagating to the surface.

Discrete element models, in common with other numerical techniques, have both advantages and disadvantages when considering their application to a geological problem of interest. On the one hand, modelling of cover deformation to high strain is an ideal candidate for the application of the discrete element technique as it is well-suited to studying problems in which discontinuities (shear-zones, faults, fractures etc) are important. It allows deformation involving unlimited relative motions of individual elements and complex, abrupt boundary conditions (Cundall and Strack, 1979; Finch et al., 2004: Egholm et al., 2007; Hardy, 2008, 2011; Thompson et al., 2010). In addition, the discrete element technique is one of the few numerical techniques which allows the formation of dilatant faults, open fractures and cavities as a natural part of the numerical scheme. In rocks such as basalts and cemented carbonates such features are of key importance (cf. Holland et al., 2006, 2011; van Gent et al., 2010; cf. Fig. 1a and b). However, one disadvantage of the technique lies in the necessary, but tedious and time-consuming, calibration of micro-particle parameters to emergent physical properties (cf. Egholm et al., 2007). Similarly, the sensitivity of models results to subtle initial differences in, e.g., assembly packing is well-known (cf. Abe et al., 2011). The interaction of many tens of thousands of particles, both locally and globally, also leads to situations wherein our ability to explain precisely why a particular fault or fracture grew at the expense of a neighbour is limited. Such issues also exist in analogue modelling of faulting where repeated experiments under the same boundary conditions are reasonably reproducible but not in the finer details of the fault and fracture systems (e.g. van Gent et al., 2010). The important scientific message to be taken from any of these studies is not the precise location of an individual fault, but rather the distinctive, repeatable patterns and sequences of structural behaviour that emerge from multiple experiments. Computational limitations on element size and/or model

resolution, whilst important previously, are now no longer a particular concern due to recent rapid advances in computational power and the parallelisation of many discrete element codes.

The scaled 2D numerical experiments reported here consider a 1.25 × 0.55 km section of the upper crust, subject to displacement on a blind, 65° normal fault centrally located at its base (Fig. 1c). Many different models have been run with parameters similar to those described below, they all had a steep basement faults (60–70°) and strength parameters of approximately the same order, within the ranges reported for natural basaltic rock masses at a metric scale. However, the specific experiment discussed herein is representative of the structural evolution typically observed in that it contains the reproducible, characteristic features seen in all the models. The model represents the cover as a densely packed assemblage of c. 47,000 variably sized, circular elements. Element radii range from 1.25 to 3.125 m (average radius 1.94 m) and their density is 2500 kg/m^3. These elements obey Newton's equations of motion and interact with normal and shear contact forces under the influence of gravity. Elements are initially bonded to their neighbours and interact elastically both in compression and tension (cf. Finch et al., 2004). Elements remain bonded until an assigned bond strain is exceeded. Bond strength is higher when subject to tangential, in comparison to normal, relative element displacement to replicate the common observation that rock masses are much stronger in compression than in tension (cf. Strayer et al., 2004). Thereafter, elements only experience non-bonded (normal elastic repulsive and tangential Mohr-Coulomb frictional) contact interactions with their neighbours (see Finch et al., 2004; Hardy et al., 2009 for a full description of the modelling approach).

In discrete element models such as that used here the bulk strength and coefficient of friction of the assemblage are emergent properties and do not relate directly to micro-properties. They are typically assessed through the use of angle of repose and unconfined/confined biaxial numerical tests (cf. Oger et al., 1998; Finch et al., 2004; Holohan et al., 2011). Using such tests, the bonded assemblage used here has been found to have a bulk coefficient of friction (μ) of c. 0.79 (internal angle of friction (ϕ) of c. 38°), a tensile strength (T) of ~0.75 MPa, a cohesion (C) of ~2.5 MPa, and an unconfined compressive strength (UCS) of ~9.0 MPa. The Young's modulus (E) of the assemblage is approximately 1.0 GPa. These values lie within the ranges reported for natural basaltic rock masses at a metric scale and are much smaller than those typically derived from centimetre-scale laboratory samples (cf. Schultz, 1996; Strayer et al., 2004; Holohan et al., 2011). Direct comparison of these model parameters with analogue studies of similar systems is difficult due to the lack of reported elastic parameters and issues around scaling (Holland et al., 2006, 2011; van Gent et al., 2010). However, the key feature of the materials used in these studies is a significant tensile strength and a cohesion that is at least double that value. In both the model presented here and these analogue studies the finite tensile strength and cohesion allow the formation of vertical-overhanging fault scarps and cavities.

Displacement on the basement fault is incremented by 0.000025 m per time-step for 6,000,000 time-steps to achieve a total displacement of 150 m (i.e. c. 5% extension). All experiments are conducted under a normal gravitational field. The simple basement displacement is transmitted directly to the cover, changing local element interactions and contact forces. As a result of this boundary displacement, the internal elements are advanced to their new positions within the model by integrating their equations of motion using Newtonian physics and a velocity-Verlet based numerical scheme (cf. Mora and Place, 1993). Element positions are saved throughout experiments to allow a detailed, high-resolution analysis of geometry, displacement and strain (cf. Cardozo and Allmendinger, 2009). The numerical code used has been parallelised using OpenMP and has been thoroughly tested and verified against the serial version (cf. Chapman et al., 2007). Typical experiments like those discussed here take ~24 h to run on a desktop machine with two 6-core Intel Xeon (X5650 – 2.66 GHz) processors.

3. Simulation results

The progressive deformation of a strong basaltic cover overlying a 65° blind normal fault will now be illustrated. This will be done by examining its geometric expression and incremental displacement magnitude (Figs. 2 and 3). For comparison, I will present results for this strong, bonded cover (representing basalt) as well as those for a weak, un-bonded, granular cover material similar to that normally used in analogue modelling studies (dry sand) to represent brittle upper-crustal rocks (e.g. Horsfield, 1977; Vendeville, 1988; McClay, 1990). This weak, granular assembly lacks any inter-particle bonding from the start of the model run – however the experiment is identical to that of the strong, bonded assembly in all other respects. For clarity, only the geometry from the central part of each experiment is shown (cf. Fig. 1c), whilst the incremental displacement magnitude field is shown across all of the experiment.

4. Strong cover experiment

Cover deformation in this experiment can be seen to evolve through a series of distinct stages as described below:

4.1. Initial deformation

From the geometry and incremental displacement magnitude field (Figs. 2 and 3), it can be seen that after the initial 10 m of displacement on the basement fault there is only minor fracturing in the cover and a gentle surface flexure/monocline has developed (Fig. 2a). At this stage, the displacement magnitude field is smooth, fan-like and radiates upwards from the blind fault tip (Fig. 3a). The cover deformation is dominantly elastic with the cover remaining essentially intact, with minor fracturing only occurring immediately around the blind fault tip and close to the surface projection of the basement fault ('A'). This fracturing is the result of bond breakage which occurs when the strength of a bond between neighbours is exceeded. Such deformation is non-recoverable and perturbs the force balance of the elements in question and their neighbours.

After 25 m displacement deformation is more strongly localised as existing fractures grow and new fractures nucleate (Fig. 2b). At the surface the monocline is still essentially intact, but is now cut by a number of these open, sub-vertical fractures particularly at its left-hand (footwall) margin (Figs. 2b and 3b) as tensile stresses develop within the upper part of the cover and bond breakage occurs. The most prominent of these fractures (labelled A) has an aperture of up to 5 m and reaches a depth of c. 100 m, note that this fracture has propagated downwards from the surface (Fig. 2a and b). The maximum dip of the flexure at this stage is 3°. The displacement magnitude field is still broadly fan-like, however the transition zone between the hanging-wall and footwall is now narrower (Fig. 3b). Both at depth and near surface, localisation is expressed as discrete jumps in displacement magnitude, although in most of the cover deformation is still continuous (Fig. 3b).

4.2. Fracture and fault growth

After 35 m fault displacement (Fig. 2c) an earlier tensile fracture (D) has propagated downwards from the surface and widened

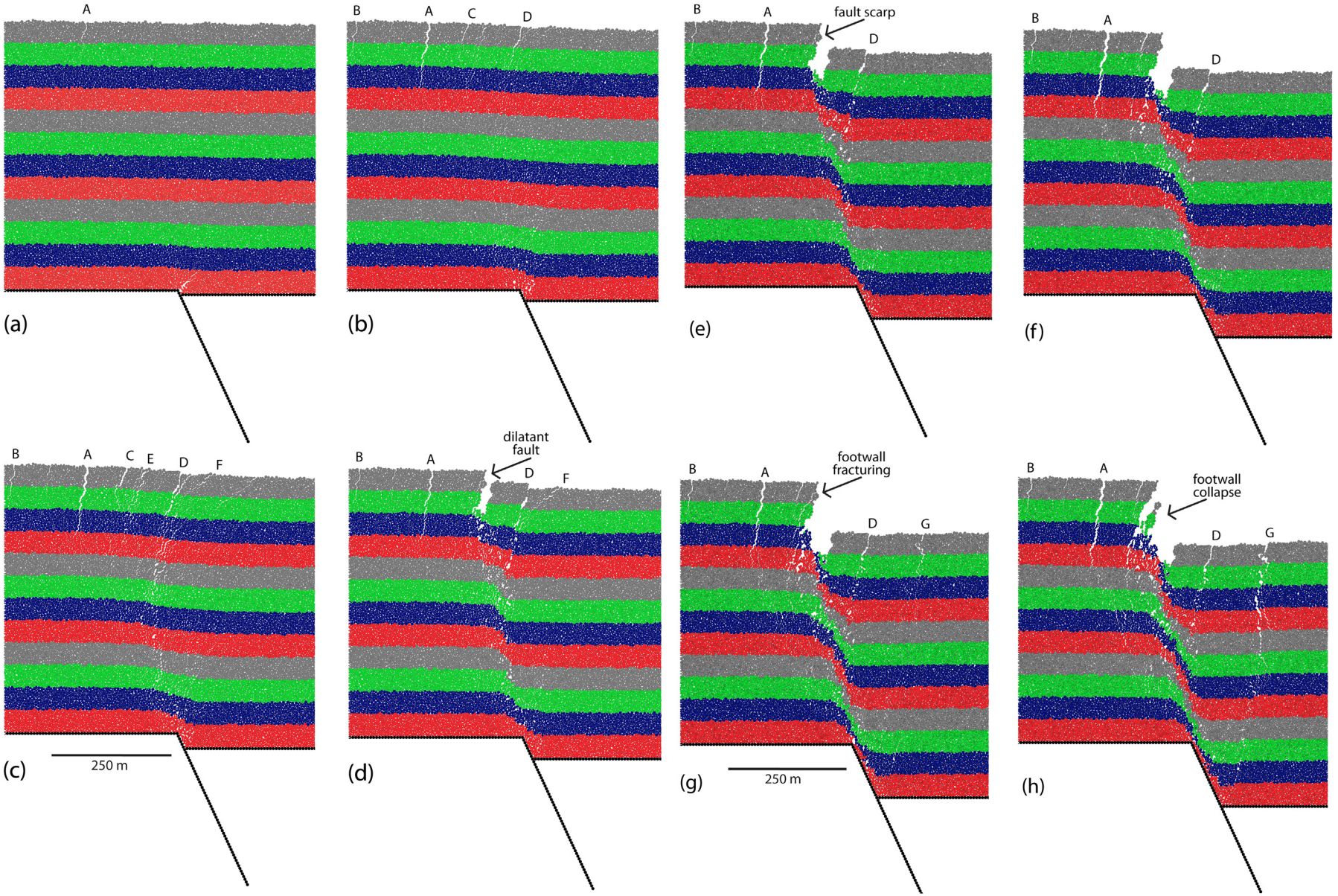

Figure 2. Evolution of bonded model geometry after (a) 10, (b) 25, (c) 35, (d) 50, (e) 75, (f) 100, (g) 125, and (h) 150 m basement fault displacement for an experiment with a basement fault dip of 65°. In the model the coloured layers are for illustration only and have no mechanical significance. Fractures and other features discussed in text are labelled, distance scale is indicated.

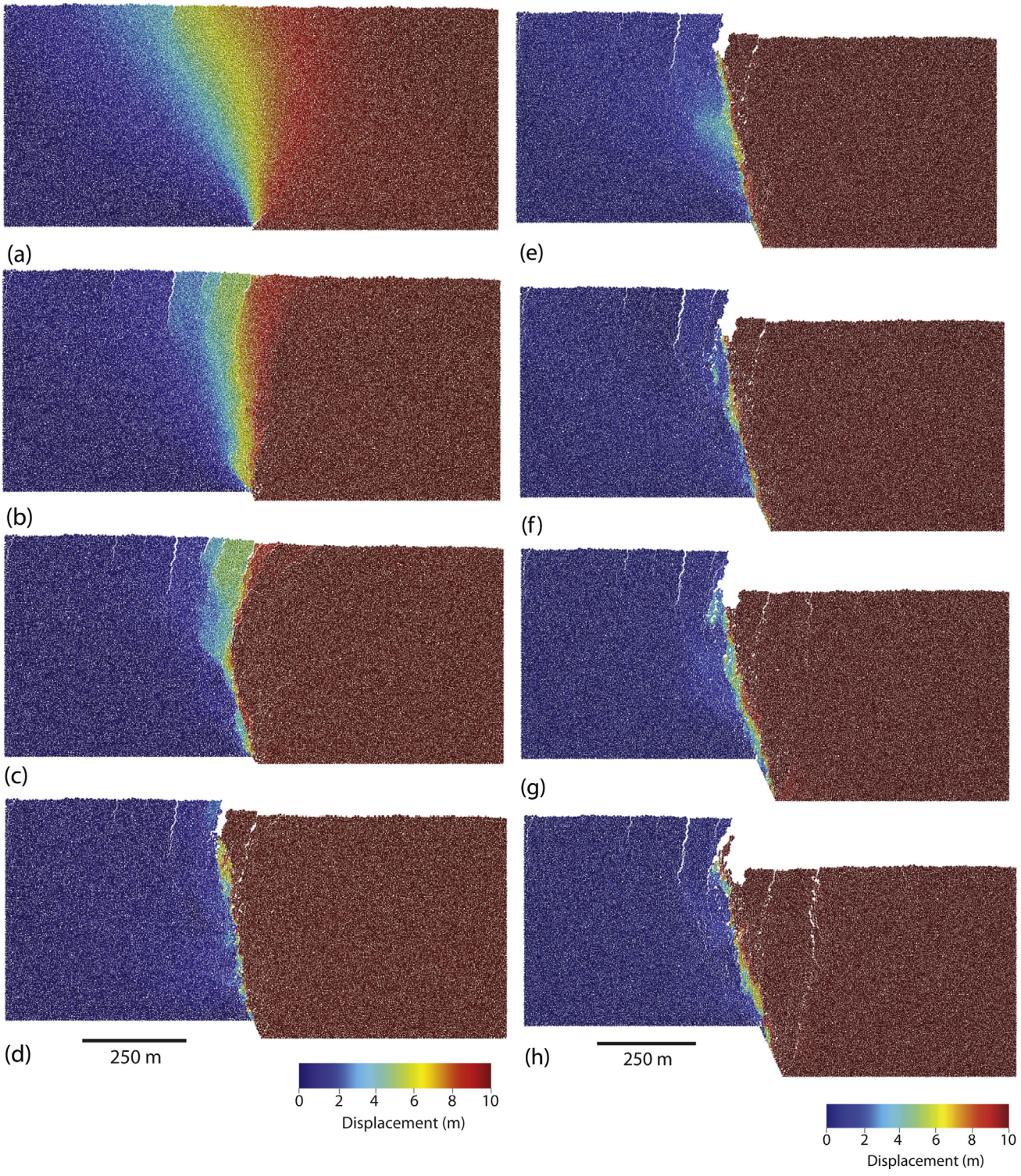

Figure 3. Evolution of incremental displacement magnitude after (a) 10, (b) 25, (c) 35, (d) 50, (e) 75, (f) 100, (g) 125, and (h) 150 m basement fault displacement for the bonded model shown in Figure 2. Displacement magnitude is calculated for each element in the cover over the previous 10 m displacement on the basement fault. Displacement magnitude scale is indicated.

producing a complex, steep, fault/fracture zone. This zone is apparently antithetic to the main fault although it has a synthetic sense of displacement. New fractures have also developed further into the hanging-wall (e.g. fracture F, Fig. 2c). The main zone of fracturing extends to c. 200 m depth. The basement fault has propagated upwards through the cover towards this fracture zone and has almost linked with it, giving the appearance of a kink in the fault zone (Figs. 2c and 3c). At this stage the open fractures and faults are beginning to disrupt the structural integrity of the monocline (Fig. 2c) whose maximum dip is now 5°. The displacement magnitude field is now much more partitioned, with discrete jumps in magnitude marking zones of localised deformation (Fig. 3c), the normal fault at depth and the zone of fracturing/faulting are particularly marked. However, there is a marked zone

of continuous (elastic) deformation in the upper part of the cover, immediately to the left of fault/fracture zone D which indicates that the cover is not yet fully breached by faulting.

4.3. Development of a through-going fault

With continued fault displacement (50 m total), the fracture labelled E becomes dominant in the upper part of the cover, develops into a dilatant fault and links with the upward propagating fault (Fig. 2d). This occurs as a result of both local and far-field force distributions and element interactions. The resultant through-going fault is a feature of all models. Most footwall and hanging-wall fractures remain open although they are now inactive, alluding to the non-recoverable nature of deformation in much of the cover. An exception is the open fracture C present at previous stages which has now closed and is no longer visible. This is a result of much of its surrounding rock mass being essentially intact, and thus elastic, when the cover was cut by the through-going fault. The through-going fault steepens from 65° at the basement fault tip to sub-vertical at the surface (Figs. 2d and 3d). The monocline is breached at the surface, producing a wedge-like structure bounded by an open, dilatant fault on its footwall margin and underlain by a zone of faulting/fracturing on its hanging-wall margin. Deformation is now localised in all of the cover (Fig. 3d).

After the next increment of displacement (75 m total) a prominent fault scarp has developed and the fault wedge structure is now clearly in the hanging-wall of the main fault (Fig. 2e). The fault is dilatant in approximately the upper 100 m of the cover, whereas at depth it is dominated by shear. The displacement magnitude field highlights the highly localised nature of deformation in the cover (Fig. 3e). During the next increment of displacement (100 m total) deformation continues in this manner (Fig. 2f). The fault at surface now has a throw of c. 70 m and an aperture of c. 40 m. The fault scarp is overhanging, un-supported and as a result shows minor fracturing prior to collapse as gravitational forces overcome the local bond strength in this region.

4.4. Footwall collapse and antithetic faulting

With further displacement (125 m total) deformation continues to be localised on the main fault but notably a new antithetic fracture (G) develops in its hanging-wall (Fig. 2g). This is due to the steeper dip of the fault (70–75°) in the cover compared with basement fault dip of 65° (cf. Holland et al., 2011), and is the first truly antithetic fracture/fault to develop in the cover. The main fault zone is complex and highly fractured with small cavities extending to depths of around 200–250 m (Fig. 2g). After the final increment of displacement (150 m total, Fig. 2h), the fault scarp has reached a height of c. 120 m and the antithetic fracture has developed into a fault with visible offset, leading to a hanging-wall which now dips gently towards the fault in contrast to all previous stages of deformation. The footwall is fractured for some distance away from the fault (e.g. open fracture A) and can be seen to be collapsing into the hanging-wall as gravitationally-induced fractures propagate downwards (Fig. 2h). The open footwall and hanging-wall fractures extend to several hundred metres depth below the model surface and commonly have surface openings of 2–5 m but can reach up to 10 m.

5. Weak cover experiment

The results of this un-bonded, frictional experiment are shown at selected, equivalent increments of displacement on the underlying fault to that of the bonded experiment (25, 50, 100 and 150 m; Fig. 4). Overall, the progressive deformation of the un-bonded cover experiment is quite distinct to that of the bonded case (compare Figs. 2 and 4; cf. Hardy, 2011). The earliest deformation takes the form of a steep-vertical fault that nucleates above the blind fault tip (labelled "V" in Fig. 4a, cf. Fig. 2b; Hardy, 2011; Nollet et al., 2012). This fault is similar to the "precursor" faults commonly reported above basement faults which can show apparent reverse offset but which are technically synthetic (cf. Horsfield, 1977; Hardy, 2011). With continued displacement, this fault is replaced progressively towards the footwall by a steep normal fault (labelled "N" in Fig. 4a and b) with a minor scarp at the surface, and finally by a normal fault which dips at an angle (c. 65°) predicted by Mohr-Coulomb theory (Fig. 4c). With further displacement and creation of topographic relief, and as the particles are un-bonded, footwall collapse occurs leading to a surface slope which tends towards the angle of repose (~35–40°) of the un-bonded material (Fig. 4c and d, cf. Fig. 2f and h). Due to the lack of tensile strength or cohesion in this cover material, the smaller-scale structures developed within it are quite distinct to those seen in the experiment with the bonded cover. In particular, it can observed that no open fractures or cavities develop in the un-bonded cover, and that the prominent fault wedge structure seen in the bonded assembly is not produced (cf. Figs. 2e and 4f). It is also notable that the fault zones in this weak, granular material are wider than those in the strong material and that surficial fault scarps are only weakly developed.

6. Discussion and conclusions

The discrete element modelling study presented here has investigated the deformation of a strong basaltic cover overlying a blind, normal fault propagating to the surface; it complements previous field, laboratory and numerical studies of similar or related systems (e.g. Horsfield, 1977; Patton and Fletcher, 1995; Finch et al., 2004; Jackson et al., 2006; Holland et al., 2006, 2011; van Gent et al., 2010; Hardy, 2011). Comparison to such studies will now be made and the implications of the work presented here assessed.

The results are strikingly similar to those seen in natural field settings, and emphasise that the occurrence of dilatant faults, open fractures and cavities/caves in extensional settings is not necessarily restricted to the very shallow section (cf. Fig. 1a; Gudmundsson, 1987; Holland et al., 2006; Acocella et al., 2003; Martel and Langley, 2006). In the strong cover experiment presented here such open fractures extend to several hundred metres depth below the model surface and commonly have surface openings of 2–5 m but can reach up to 10 m. While such fracture apertures are large, they can be compared to those of Acocella et al. (2003) and Grant and Kattenhorn (2004) both of whom report common openings of around 2 m but with some examples reaching 10–20 m. In the numerical model the aperture of the through-going dilatant fault at surface can reach up to 40 m; Gudmundsson (1987) and Grant and Kattenhorn (2004) report comparable fault apertures from the Thingvellir fissure swarm in Iceland with maximum values of 50–70 m (cf. Fig. 1a). Thus, it can be proposed that the basic geometries of the dilatant structures seen in these experiments are broadly comparable with those seen in natural examples (cf. Gudmundsson, 1987; Holland et al., 2011), although the detailed geometries of the fractures/faults/cavities at scales approaching model resolution may not directly correspond to features we see in nature. Of particular interest are the vertical to near-vertical fault scarps on surface-breaking faults that are clearly dilational (with both opening and vertical displacements) documented in basalts from around the world (e.g. Gudmundsson, 1987; Acocella et al., 2003; Holland et al., 2006; Ferrill et al., 2011). There has been much discussion on the manner in which such faults

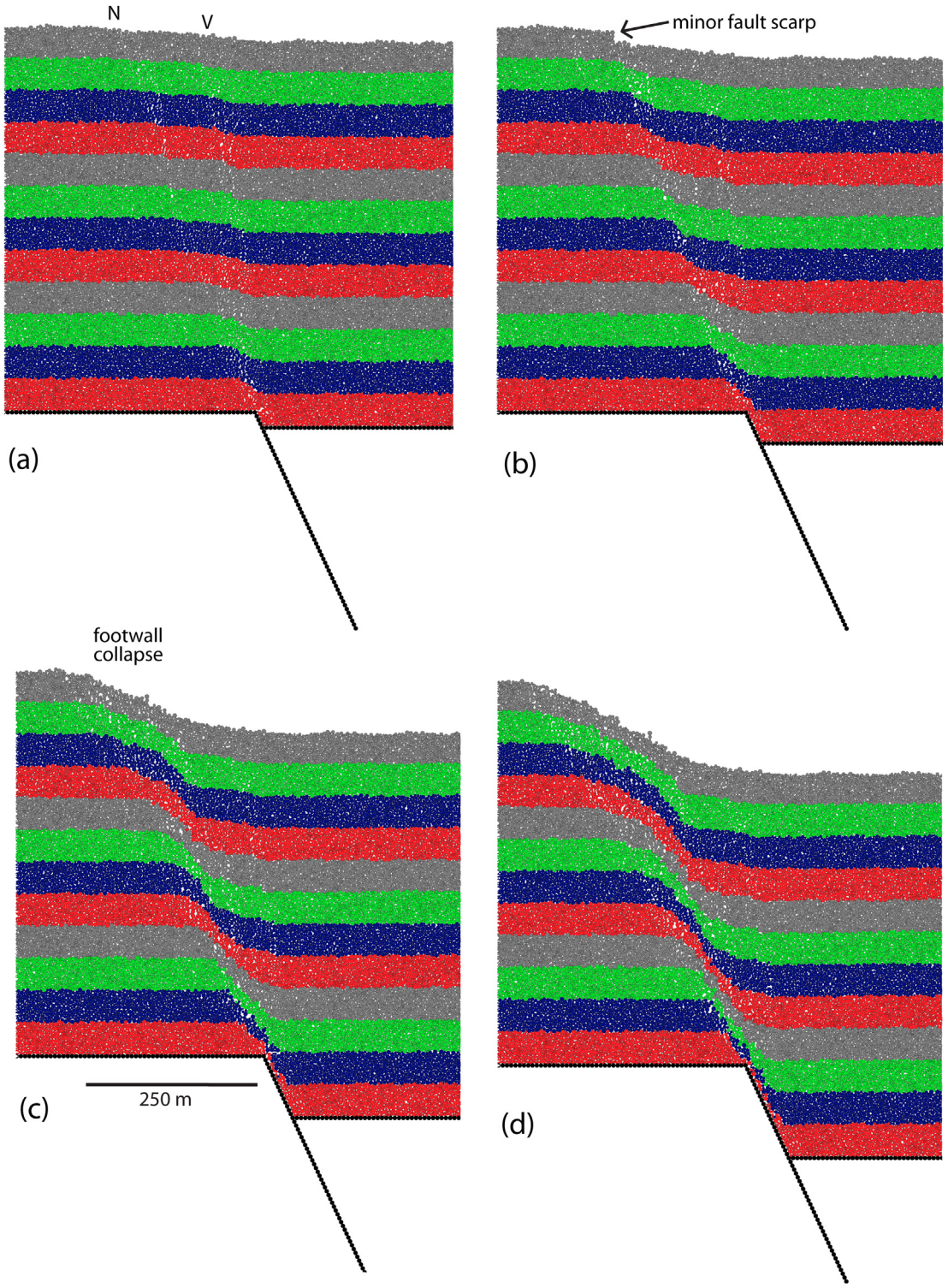

Figure 4. Evolution of un-bonded model geometry after (a) 25, (b) 50, (c) 100, and (d) 150 m basement fault displacement for an experiment with a basement fault dip of 65°. All other parameters are identical to the model shown in Figure 2. In the model coloured layers are for illustration only and have no mechanical significance. Distance scale is indicated.

initiate and grow, some authors advocating that open surface fractures propagate downwards and develop into faults (Acocella et al., 2003), while others favour a model in which a blind fault propagates upwards (Grant and Kattenhorn, 2004). A comparison with the through-going fault developed in the experiment presented here is thus appropriate. At surface this fault is vertical to overhanging, has significant throw, is massively dilatant and yet has fault surfaces that were never in frictional contact (e.g. Fig. 2f). This part of the fault initiated as a surface tension fracture (compare Figs 2c and e). In contrast, at depth the fault shallows to link with the basement fault, has no aperture and displacement is accommodated primarily by shear. Thus, the model results presented here suggest that a conceptual model involving the linkage of a downward propagating open fracture and an upward propagating shear fault is perhaps more appropriate to explain field observations (cf. Fig. 5 below).

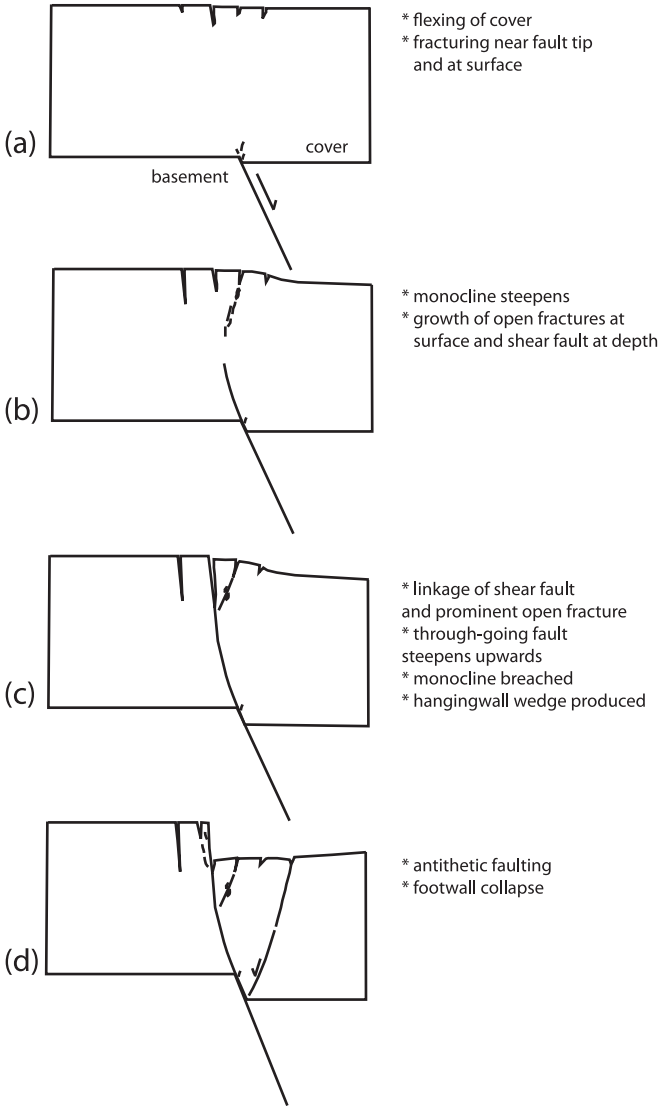

Figure 5. Schematic, conceptual fault growth model in basalt cover integrating both the numerical results presented here and analogue modelling studies with comparable materials and boundary conditions (Holland et al., 2006, 2011). An evolution from (a) a monoclinal structure, with open fractures at the surface, through fault-propagation from depth and downward propagation of open fractures (b and c), to a steep through-going fault and subsequent antithetic faulting (d) is a common theme in all these studies.

The simulation results presented here are also similar to published studies of analogue experiments with broadly similar material properties and boundary conditions (e.g. Holland et al., 2006; van Gent et al., 2010; Holland et al., 2011; cf. Fig. 1b and c). In all of these studies dilatant faults, open fractures, antithetic fractures, ramps, fault wedges and collapse structures are reported and are similar to those seen here. A direct comparison can be made with the results and conclusions of Holland et al. (2006, 2011). In both these studies an evolutionary sequence very similar to that seen in the bonded experiment presented here was observed (cf. Figs. 2 and 5). A summary, conceptual, fault growth model integrating results from both analogue modelling results and the numerical results presented here is given in Figure 5. The key factor in producing such a model response appropriate to basalts (or cemented carbonates) is the correct choice of analogue or numerical model materials; simple granular, frictional materials clearly are not adequate for modelling such strong, intact, rocks at shallow depths. The numerical results presented here illustrate this well and emphasise that when attempting to numerically model the structures seen in strong, near-surface materials the inclusion of a tensile strength/cohesion in the model material is paramount (cf. Figs. 2 and 4).

Here I have also shown the applicability of the discrete element technique to modelling strong, basaltic materials overlying large, blind normal faults. It is particularly appropriate for examining their behaviour and expression at large displacements when the fault becomes through-going and has prominent surface expression. Many of the features produced in both analogue models and the discrete element model under such conditions are difficult to reproduce using continuum techniques. However, this is not to say that such continuum techniques do not give valuable insights into fault growth in the crust, but rather that scientific questions asked at different scales perhaps require different approaches. Such continuum numerical models have been predominantly applied at lithospheric scales to problems such as rift initialisation and localization (e.g., Burov and Poliakov, 2001; Buck et al., 2003). They give more fundamental insight into why and when crustal normal faults localise at particular locations but do not provide the finer scale details in the upper c. 1 km of the crust that are of concern here.

In summary, while the present-day surface morphology and structure of normal faults in basalts is often visible and spectacular in nature (e.g., Acocella et al., 2003; Grant and Kattenhorn, 2004; Holland et al., 2006; Martel and Langley, 2006; Ferrill et al., 2011; Fig. 1a), their deeper geometry is typically obscured and/or difficult to interpret. The results presented here may provide some useful templates for the interpretation and/or restoration of field and seismic data in such settings and highlight some key features:

- Deformation of basalts above blind, normal faults is complex: open fractures, cavities, fault wedges, dilational and shear faults can all develop, reflecting both the strong, brittle nature of basalt near the Earth's surface and the low mean effective stress in such settings.
- Deformation follows a predictable evolution: an initial elastic stage of deformation produces a very gentle monoclinal flexure. This is followed by the development of sub-vertical Mode 1 fractures at the surface and a shear fault at depth. Simultaneously, a series of hanging-wall fractures develop in the upper part of the cover. With continued displacement, surface fractures propagate downwards, whilst the fault at depth propagates upwards. The monocline is then cut by open fractures on its footwall and hanging-wall margins leaving a remnant, fault-wedge structure. Finally, a prominent open

fracture and deeper fault link, forming a through-going structure. The upward-steepening nature of the master fault causes late antithetic faulting in the hanging-wall at large displacements. This pattern also occurs in analogue modelling studies using comparable materials (Holland et al., 2006, 2011; Figs. 1b and 5).

- The application of standard kinematic/geometric forward modelling or restoration techniques to such structures is problematic as deformation is neither simple nor continuous. Any technique applied must take into account open fractures and faults with significant apertures.

Finally, while no attempt has been made to specifically model individual structures, the strong similarity between analogue models, outcrop examples and the numerical experiments presented here gives us confidence in the ability of the model to simulate intact, strong materials under these and more complicated boundary conditions. While the model presented here appears to be a robust simulator of elastic-brittle materials with tensile and cohesive strength, one must always bear in mind that the detailed geometries of fractures at scales approaching model resolution may not directly correspond to features seen in nature. The results presented here are most applicable to settings in which blind normal faults are an important feature and where there is a strong brittle cover. Thus, while the material properties and geological setting might vary somewhat, the broad implications of this work can be applied to cemented carbonates as well (e.g. van Gent et al., 2010). Clearly, modelling the cover as a simple homogeneous, strong, material is a simplification; variable mechanical stratigraphy is an important factor in many natural structures, leading to complex juxtapositions of deformation mechanisms and styles. Strongly mechanically-layered cover stratigraphies have been shown to produce complex hanging-wall and footwall geometries in sedimentary sequences (cf. Sharp et al., 2000; Egholm et al., 2008; van Gent et al., 2010), one can imagine that similar mechanical stratigraphies may also exist in basaltic sequences due to the interlayering of tuffs or weathered horizons. Nevertheless, the modelling results presented here show that even with simple boundary conditions and a homogeneous cover sequence, complex structural relationships can be produced. Finally, real faults are three-dimensional structures and clearly a 3D model would allow a more complete analysis. These and other topics are the subjects of ongoing research.

Acknowledgements

Discussions with, and the patience of, many colleagues over many years is appreciated; in particular Rick Allmendinger, Nestor Cardozo, Josep Anton Muñoz, Eduard Roca, Ken McClay and Dave Waltham are thanked. The comments of 2 anonymous referees have greatly improved this manuscript. HMS and JMS are thanked for bringing colour into my life. This research is supported by ICREA, the STAR consortium, the Geomodels programme, and the Seismic Imaging of Fault Zones project funded by NFR.

References

Abe, S., van Gent, H., Urai, J.L., 2011. DEM simulation of normal faults in cohesive materials. Tectonophysics 512, 12–21.
Acocella, A., Korme, T., Salvini, F., 2003. Formation of normal faults along the axial zone of the Ethopian Rift. Journal of Structural Geology 25, 503–513.
Allmendinger, R.W., 1998. Inverse and forward numerical modeling of trishear fault propagation folds. Tectonics 17, 640–656.
Buck, W.R., Lavier, L., Babeyko, A., 2003. A numerical model of lithospheric extension producing fault-bounded basins and ranges. International Geology Review, 712–723. http://dx.doi.org/10.2747/0020-6814.45.8.712.
Burov, E., Poliakov, A., 2001. Erosion and rheology controls on synrift and postrift evolution: verifying old and new ideas using a fully coupled numerical model. Journal of Geophysical Research 106 (B8), 16461–16481. http://dx.doi.org/10.1029/2001JB000433.
Cardozo, N., Allmendinger, R.W., 2009. SSPX: a program to compute strain from displacement/velocity data. Computers & Geosciences 35, 1343–1357.
Chapman, B., Jost, G., van der Pas, R., 2007. Using OpenMP: Portable Shared Memory Parallel Programming. The MIT Press.
Clifton, A.E., Schlische, R.W., 2003. Fracture populations on the Reykjanes Peninsula, Iceland: comparisons with experimental clay models of oblique rifting. Journal of Geophysical Research 108 (B2), 17. http://dx.doi.org/10.1029/2001JB000635.
Crook, A., Wilson, S., Yu, J., Owen, D., 2006. Predictive modelling of structure evolution in sandbox experiments. Journal of Structural Geology 28, 729–744.
Cundall, P.A., Strack, O.D.L., 1979. A discrete numerical model for granular assemblies. Geotechnique 29, 47–65.
Dooley, T.P., McClay, K.R., Pascoe, R., 2003. 3D analogue models of variable displacement extensional faults: applications to the Revfallet fault systems, Mid-Norway. In: Nieuland, D.A. (Ed.), New Insights into Structural Interpretation and Modelling, Geological Society of London Special Publication, vol. 212, pp. 151–167.
Egholm, D.L., Sandiford, M., Clausen, O.R., Nielsen, S.B., 2007. A new strategy for discrete element numerical models: 2. Sandbox applications. Journal of Geophysical Research 112, B05204. http://dx.doi.org/10.1029/2006JB004558.
Egholm, D.L., Clausen, O.R., Sandiford, M., Kristensen, M.B., Korstgård, J.A., 2008. The mechanics of clay smearing along faults. Geology 36, 787–790.
Ferrill, D., Wyrick, D.Y., Smart, K.J., 2011. Coseismic, dilational-fault and extensional fracture related pit chain formation in Iceland: analog for pit chains on Mars. Lithosphere 3, 133–142.
Finch, E., Hardy, S., Gawthorpe, R.L., 2004. Discrete element modelling of extensional fault-propagation folding above rigid basement fault blocks. Basin Research 16, 489–506.
Gawthorpe, R.L., Sharp, I., Underhill, J.R., Gupta, S., 1997. Linked sequence stratigraphic and structural evolution of propagating normal faults. Geology 25, 795–798.
Grant, J.V., Kattenhorn, S.A., 2004. Evolution of vertical faults at an extensional plate boundary, southwest Iceland. Journal of Structural Geology 26, 537–557.
Gray, J.P., Monaghan, J.J., 2004. Numerical modelling of stress fields and fracture around magma chambers. Journal of Volcanology and Geothermal Research 135, 259–283.
Gudmundsson, A., 1987. Tectonics of the Thingvellir fissure swarm, SW Iceland. Journal of Structural Geology 9, 61–69.
Hardy, S., 2008. Structural evolution of calderas: insights from two-dimensional discrete element simulations. Geology 36, 927–930.
Hardy, S., 2011. Cover deformation above steep, basement normal faults: insights from 2D discrete element modeling. Marine and Petroleum Geology 28, 966–972.
Hardy, S., McClay, K.R., 1999. Kinematic modelling of extensional fault-propagation folding. Journal of Structural Geology 21, 695–702.
Hardy, S., McClay, K., Muñoz, J.A., 2009. Deformation and fault activity in space and time in high-resolution numerical models of doubly vergent thrust wedges. Marine and Petroleum Geology 26, 232–248. http://dx.doi.org/10.1016/j.marpetgeo.2007.12.003.
Holland, M., 2004. Structure of Fault Zones in Cohesive Volcanic Sequences (Diploma thesis at the RWTH Aachen).
Holland, M., Urai, J., Martel, S., 2006. The internal structure of fault zones in basaltic sequences. Earth and Planetary Science Letters 248, 286–300.
Holland, M., van Gent, H., Bazalgette, L., Yassir, N., Hoogerduijn Strating, E.H., Urai, J.S., 2011. Evolution of dilatant fracture networks in a normal fault – evidence from 4D model experiments. Earth and Planetary Science Letters 304, 399–406.
Holohan, E.P., Schopfer, M.P.J., Walsh, J.J., 2011. Mechanical and geometric controls on the structural evolution of pit crater and caldera subsidence. Journal of Geophysical Research 116, B07202. http://dx.doi.org/10.1029/2010JB008032.
Horsfield, W.T., 1977. An experimental approach to basement-controlled faulting. Geologie en Mijnbouw 56, 363–370.
Jackson, C.A.L., Gawthorpe, R.L., Sharp, I.R., 2006. Style and sequence of deformation during extensional fault-propagation folding: examples from the Hammam Faraun and El-Qaa fault blocks, Suez Rift, Egypt. Journal of Structural Geology 28, 519–535.
Jin, G., Groshong, R.H., 2006. Trishear kinematic modeling of extensional fault-propagation folding. Journal of Structural Geology 28, 170–183.
Jónsson, S., 2008. Importance of post-seismic viscous relaxation in southern Iceland. Nature Geoscience 1, 136–139. http://dx.doi.org/10.1038/ngeo105.
Kaven, J.O., Martel, S.J., 2007. Growth of surface-breaching normal faults as a three-dimensional fracturing process. Journal of Structural Geology 29, 1463–1476.
Leeder, M.R., Seger, M.J., Stark, C.P., 1991. Sedimentation and tectonic geomorphology adjacent to major active and inactive normal faults, southern Greece. J. Geol. Soc. London 148, 331–343.
McClay, K.R., 1990. Extensional fault systems in sedimentary basins: a review of analogue model studies. Marine and Petroleum Geology 7, 206–233.
Mandl, G., 2000. Faulting in Brittle Rocks: an Introduction to the Mechanics of Tectonic Faults. Springer, Berlin, Germany, p. 434.
Martel, S.J., Langley, J.S., 2006. Propagation of normal faults to the surface in basalt, Koae fault system, Hawaii. Journal of Structural Geology 28, 2123–2143.

Mora, P., Place, D., 1993. A lattice solid model for the non-linear dynamics of earthquakes. International Journal of Modern Physics C 4, 1059–1074.
Nollet, S., Kleine Vennekate, G.J., Giese, S., Vrolijk, P., Urai, J.L., Zeigler, M., 2012. Localization patterns in sandbox-scale numerical experiments above a normal fault in basement. Journal of Structural Geology 39, 199–209.
Oger, L., Savage, S.B., Corriveau, D., Sayed, M., 1998. Yield and deformation of an assembly of disks subject to a deviatoric stress loading. Mechanics of Materials 27, 189–210.
Patton, T.L., Fletcher, R.C., 1995. Mathematical block-motion model for deformation of a layer above a buried fault of arbitrary dip and sense of slip. Journal of Structural Geology 17, 1455–1472.
Saltzer, S.D., Pollard, D.D., 1992. Distinct element modeling of structures formed in sedimentary overburden by extensional reactivation of basement normal faults. Tectonics 11, 165–174.
Schultz, R.A., 1996. Relative scale and the strength and deformability of rock masses. Journal of Structural Geology 18, 1139–1149.
Sharp, I.R., Gawthorpe, R.L., Underhill, J.R., Gupta, S., 2000. Fault propagation folding in extensional settings: examples of structural style and syn-rift sedimentary response from the Suez Rift, Egypt. Geological Society of America Bulletin 112, 1877–1899.
Smart, K.J., Ferrill, D.A., Morris, A.P., Bichon, B.J., Riha, D.S., Huyse, L., 2010. Geomechanical modeling of an extensional fault-propagation fold: Big Brushy Canyon monocline, Sierra Del Carmen, Texas. American Association of Petroleum Geologists Bulletin 94, 221–240.
Strayer, L.M., Erickson, S.G., Suppe, J., 2004. Influence of growth strata on the evolution of fault-related folds: distinct-element models. In: McClay, K. (Ed.), Thrust Tectonics and Hydrocarbon Systems, American Association of Petroleum Geologists Memoir, vol. 82, pp. 413–437.
Thompson, N., Bennett, M.R., Petford, N., 2010. Development of characteristic volcanic debris avalanche deposit structures: new insights from distinct element simulations. Journal of Volcanology and Geothermal Research 192, 191–200.
van Gent, H.W., Holland, M., Urai, J.L., Loosveld, R., 2010. Evolution of fault zones in carbonates with mechanical stratigraphy – insights from scale models using layered cohesive powder. Journal of Structural Geology 32, 1375–1391.
Vendeville, B.C., 1988. Scale-models of basement induced-extension. Comptes Rendus de l'Académie des Sciences 307, 1013–1019.
Villemin, T., Bergerat, F., 2013. From surface fault traces to a fault growth model: the Vogar Fissure Swarm of the Reykjanes Peninsula, Southwest Iceland. Journal of Structural Geology 51, 38–51.
White, N.J., Jackson, J.A., McKenzie, D.P., 1986. The relationship between normal faults and that of sedimentary layers in their hangingwalls. Journal of Structural Geology 8, 897–910.
Willsey, S.P., Umhoefer, P.J., Hilley, G.E., 2002. Early evolution of an extensional monocline by a propagating normal fault: 3D analysis from combined field study and numerical modeling. Journal of Structural Geology 24, 651–669.
Withjack, M.O., Olsen, J., Petersen, E., 1990. Experimental models of extensional forced folds. AAPG Bulletin 74, 1038–1054.
Withjack, M.O., Schlische, R.W., 2006. Geometric and experimental models of extensional fault-bend folds. In: Buiter, S.J.H., Schreurs, G. (Eds.), Analogue and Numerical Modelling of Crustal-scale Processes, Geological Society, London, Special Publications, vol. 253, pp. 285–305.